EIGHTEENTH EUROPEAN ROTORCRAFT FORUM

B - 04

Paper No 57

VALIDATION OF A BOUNDARY INTEGRAL FORMULATION FOR THE AERODYNAMIC ANALYSIS OF ROTORS IN FORWARD FLIGHT

P. RENZONI, A. VISINGARDI, A. PAGANO
C.I.R.A., ITALY

September 15 - 18, 1992

AVIGNON, FRANCE

ASSOCIATION AERONAUTIQUE ET ASTRONAUTIQUE DE FRANCE

VALIDATION OF A BOUNDARY INTEGRAL FORMULATION FOR THE AERODYNAMIC ANALYSIS OF ROTORS IN FORWARD FLIGHT

P. Renzoni, A. Visingardi, and A. Pagano

CIRA, Centro Italiano Ricerche Aerospaziali
81043 Capua, Italy

ABSTRACT

A boundary integral formulation for helicopter rotor aerodynamics is validated both in nonlifting and lifting forward flight conditions. In nonlifting conditions the formulation is compared to a finite difference code. The method gives accurate results in the linear flow regime. In lifting conditions, induced velocities on a plane approximately one chord above the tip-path-plane are compared to experiment and to an industrial lifting-line rotor code. There is good agreement with experimental data where fuselage effects are small. Similarities between the lifting-line rotor code and the incompressible version of the boundary integral formulation indicates that classical lifting-line rotor codes may not be "fully" compressible.

1. INTRODUCTION

The comprehensive analysis of the helicopter main rotor in forward flight requires the coupling of blade aerodynamics (with a complex wake system), dynamics, elastic properties, and fuselage effects. With current computers only lifting-line theory, which depends on airfoil tables and corrections for unsteady flow, has been integrated in comprehensive analysis codes. In view of ever increasing computer resources, more accurate aerodynamic analyses need to be developed that greatly reduce the dependence on airfoil tables and on corrections to account for various flow phenomena (*i.e.* unsteady flow, yawed or swept flow, tip flow, dynamic stall, etc.) and that properly models the rotor wake structure.

A general review of the integral equation methods developed over the past twenty years can be found in Morino and Tseng [1] along with the development of the direct boundary element formulation for the velocity potential. In recent years, Morino and his collaborators at the University of Rome "La Sapienza" have developed a boundary integral formulation for bodies in arbitrary rigid-body motion [2,3]. The formulation was found to be easier to derive and to apply than that presented in [1]. It can be applied to any number of bodies that move in rigid-body motion with respect to each other. This is ideal for helicopter aerodynamics since the main rotor, tail rotor, fuselage and empennages, and wakes can be treated using a single formulation.

A brief overview of the formulation is given in the next section for a non-articulated rotor in forward flight. Those interested in a more complete treatment of the theory may refer to [2,3]. A method for treating articulated rotors is also discussed in the next section. The validation is carried out on nonlifting and lifting test cases. Comparisons are made both with experimental data and with other numerical formulations.

2. INTEGRAL FORMULATION

The governing equation for potential compressible flows, written in an air frame of reference (AFR, fixed with the undisturbed air), is given by

$$\nabla_\xi{}^2\phi - \frac{1}{a_\infty^2}\frac{\partial^2\phi}{\partial\tau^2} = \sigma \qquad \boldsymbol{\xi} \text{ outside } S(\tau) \tag{1}$$

where ϕ is the velocity potential such that $\mathbf{v} = \nabla_\xi\phi$ and σ indicates the nonlinear terms that are important only in transonic regime. $S(\tau)$ is a surface outside of which the flow is potential and it consists of a surface S_B surrounding the blades and a surface S_W surrounding the wake. The boundary condition at infinity is that $\phi = 0$. The surface S_B of the blade is assumed to be impermeable hence $\partial\phi/\partial n = \mathbf{v}_B \cdot \mathbf{n}$ where $\mathbf{v}_B$ is the velocity of a point on the blades. The wake is a surface of discontinuity which is not penetrated by the fluid and across which there is no pressure jump. The second wake condition implies that $\Delta\phi$ remains constant following a wake point $\mathbf{x}_W$, and equal to the value it had when $\mathbf{x}_W$ left the trailing edge. The value of $\Delta\phi$ at the trailing edge is obtained by using the Kutta-Joukowski hypothesis that no vortex filament exists at the trailing edge; this implies that the value of $\Delta\phi$ on the wake and the value of $\Delta\phi$ on the body are equal at the trailing edge.

Applying the Green's function method to Eq. (1), neglecting the nonlinear terms ($\sigma = 0$), yields the following boundary-integral-representation for the velocity potential ϕ

$$E(\mathbf{x}_*)\phi(\mathbf{x}_*, t_*) = I_B + I_W \tag{2}$$

with

$$\begin{aligned} I_B &= \iint_{S_B} \left\{ \frac{-1}{4\pi\hat{\varrho}}\frac{\partial\phi}{\partial\tilde{n}} - \phi\left[\frac{\partial}{\partial\tilde{n}}\left(\frac{-1}{4\pi\hat{\varrho}}\right) + \frac{-1}{4\pi\hat{\varrho}}\frac{\partial}{\partial t}\left(\mathrm{M}\cdot\mathbf{n}\mathrm{M}\cdot\nabla\theta - \frac{\mathrm{M}\cdot\mathbf{n}}{a_\infty}\right)\right] \right. \\ &+ \left. \frac{-1}{4\pi\hat{\varrho}}\left(\frac{\partial\theta}{\partial\tilde{n}} + 2\frac{\mathrm{M}\cdot\mathbf{n}}{a_\infty}\right)\frac{\partial\phi}{\partial t}\right\}_{t_*-\theta} dS \end{aligned} \tag{3}$$

and

$$I_W = \iint_{S_{W_t}} \left\{\frac{\partial}{\partial n}\left(\frac{-1}{4\pi\varrho}\right)\Delta\phi\right\}_{t_*-\varrho/a_\infty} dS + \int_{L_{W_t}} \left\{\Omega\frac{1}{4\pi\varrho}\mathbf{a}_\lambda \times \mathbf{a}_\alpha \cdot \nabla_{\xi_*}\theta\Delta\phi\right\}_{t_*-\varrho/a_\infty} d\lambda \tag{4}$$

where $E(\mathbf{x}_*)$ is a domain function defined as zero inside S and unity everywhere else. Furthermore, $\partial/\partial\tilde{n} = \partial/\partial n - \mathrm{M}\cdot\mathbf{n}\mathrm{M}\cdot\nabla$, $\hat{\varrho} = [\varrho|1 + \mathrm{M}\cdot\boldsymbol{\varrho}/\varrho|]_{t_*-\theta}$, and $\varrho = ||\boldsymbol{\varrho}|| = ||\boldsymbol{\xi} - \boldsymbol{\xi}_*||$ (where $\boldsymbol{\xi}$ is the position occupied in the AFR by a point $\mathbf{x}$ of the moving frame of reference, at time t, and $\boldsymbol{\xi}_*$ is the position occupied in the AFR by a point $\mathbf{x}_*$ of the moving frame of reference, at time t_*). For a rigid non-articulated rotor, the local Mach number is given by $\mathrm{M} = (\Omega \times \mathbf{x} + \mathrm{R}_\psi^T(t)\mathbf{v}_T)/a_\infty$ in which R_ψ represents a uniform rotation matrix about the z-axis. with angular velocity Ω, $\mathbf{v}_T$ is the translational velocity.

In the above formulation each surface integral is expressed in a frame of reference fixed with the surface of integration itself, thereby simplifying the formulation and the evaluation of the integrals. Equation (3) is expressed in a body frame of reference (BFR, fixed to the blades moving in rigid-body motion) and is obtained from the differential equation in the BFR. The integrals are evaluated at $t = t_* - \theta$ where $\theta = \hat{\varrho}/a_\infty$ is the time required for a signal emitted in $\mathbf{x}$ to arrive in $\mathbf{x}_*$. Equation (4) is expressed in the AFR, where the wake surface is a time-independent function. The potential at a point $\boldsymbol{\xi}_*$ on the rotor at time t_* is influenced by signals emitted from points on the wake generated at or before the delay time $t_D = t_* - \varrho(\boldsymbol{\xi}_*, \boldsymbol{\xi})/a_\infty$. Wake points generated after time t_D have no influence and are excluded from the integration. The wake contribution is written in terms of a surface integral over S_{W_t}, the portion of the wake influencing the point $\boldsymbol{\xi}_*$ on the rotor, and a line integral on L_{W_t}, the line delimiting the zone of influence. The line L_{W_t} represents the location of the trailing edge point, $\mathbf{x}_{TE}$, at the istant $t = t_* - \theta$ when the signal was emitted.

Also, $\mathbf{a}_\lambda$ and $\mathbf{a}_\alpha$ are the covariant base vectors of the λ, α coordinate system over S_W in which λ is the distance from the instantaneous axis of rotation and α is the azimuthal position of a wake point.

If $\mathbf{x}_*$ is a smooth point on S_B, Eq. (2) represents a compatability condition between the values of ϕ and $\partial\phi/\partial\tilde{n}$ on S_B, and $\Delta\phi$ on the surface of the wake, S_W. $\partial\phi/\partial\tilde{n}$ is known from the impermeability condition on the rotor and $\Delta\phi$ on the wake is known from the previous time step. This compatibility condition yields an integral equation that is used to evaluate ϕ on S_B.

This formulation has been extended to an articulated rigid rotor by introducing the appropriate boundary conditions on the rotor. The blade motion is expressed in a Fourier series for pitching and flapping. On the blades $\partial\phi/\partial n = \mathbf{v}_B \cdot \mathbf{n}$ where

$$\mathbf{v}_B = \mathbf{v}_T + \left[\dot{\mathbf{R}}_\psi \cdot \mathbf{R}_\beta \cdot \mathbf{R}_\theta + \mathbf{R}_\psi \cdot \dot{\mathbf{R}}_\beta \cdot \mathbf{R}_\theta + \mathbf{R}_\psi \cdot \mathbf{R}_\beta \cdot \dot{\mathbf{R}}_\theta\right] \cdot \mathbf{x}_B \tag{5}$$

in which $\mathbf{R}$ represent the rotation matrices and $\dot{\mathbf{R}}$ their time derivatives.

A zeroth-order boundary element method (BEM) is used for the discretization of the integral equation, Eq. (2). The surface of the rotor and of the wake are divided into hyperboloidal quadrilateral elements and ϕ, $\partial\phi/\partial\tilde{n}$, $\Delta\phi$ are assumed constant over each element. Using the collocation method and setting the collocation points at the centroid of each element on the rotor, leads to a differential-delay equation for the velocity potential ϕ which in matrix form is

$$[\mathbf{A}]\{\phi\} = \{\mathbf{b}\} \tag{6}$$

where $[\mathbf{A}]$ is the matrix of influence coefficients at the current time t, $\{\phi\}$ is the vector of unknown velocity potentials, and $\{\mathbf{b}\}$ is a vector of terms known at time t. The elements of $[\mathbf{A}]$ and $\{\mathbf{b}\}$ are calculated analytically. The above system of simultaneous linear algebraic equations is solved for the unknown vector $\{\phi\}$ at each time step by inverting $[\mathbf{A}]$.

3. RESULTS AND DISCUSSION

The integral formulation presented in the previous section, due to its recent development, has not been extensively validated. Tests have been conducted by Morino et al. [2,3] on a one-bladed configuration with a collective pitch of 5.7°. Comparisons with a lifting surface theory [4] and with another boundary integral formulation [1] showed discrepancies in terms of the magnitude of the thrust coefficient when the blade was advancing, although all methods showed a similar behavior. When the blade was retreating, the present formulation agreed well with the lifting surface theory. A series of tests have been performed in order to assess the ability of the present formulation to predict the pressure distribution on the blade and to capture flowfield details.

3.1 *Nonlifting Test Case*

The ideal case of a nonlifting rotor (symmetric, non-twisted blade at zero angle of attack) is generally used in the validation of finite difference codes that cannot treat rotor wakes. In our case, it will be used to determine the surface discretization (blade paneling) required to obtain an accurate pressure distribution. It will also give an indication of the limits of the integral formulation in supercritical flow regions. Comparisons are made with experimental data from a model rotor that was tested at ONERA in 1978 [5] and with a finite difference rotor code [6] that has been tested extensively on the same data. Experimental pressure distributions are available only in the blade tip region of the advancing blade. For this reason most of the comparisons are made with the finite difference code. The finite difference code solves the unsteady full potential equation in nonconservative form written in a blade-attached moving frame of reference.

The two-bladed model rotor is 1.5 m in diameter. The blade has a trapezoidal planform and the airfoil section varies from a NACA 0017 at the root to a NACA 0009 at the tip. The results presented here are for an advance ratio of 0.4 and a tip Mach number of 0.624.

Figure 1 shows the general behavior of the present formulation (BEM) with respect to the finite difference code (FDM). The iso-pressure coefficient lines clearly indicate the regions on the blade that approach supercritical conditions. At $\psi = 30°$ the two methods agree quite well while at $\psi = 60°$ there is a first indication of a shock at the blade tip that is clearly not captured by the present method. As expected, the greatest difference between the two methods occurs at $\psi = 120°$ where a strong shock appears. Nevertheless, there is still good agreement over most of the blade where the flow is linear. At $\psi = 150°$ there is good agreement over the entire blade. The integral method uses 36 panels in the chordwise direction and 15 panels in the spanwise direction while the finite difference code uses a 93×21 surface grid. Despite the coarse discretization used, accurate results are obtained in linear flow regions. At an azimuth position of $\psi = 120°$ there is very good agreement at an internal station, $r/R = 0.47$, in terms of pressure coefficient (Fig. 2a). However, toward the blade tip, $r/R = 0.89$, the linear integral method cannot handle the onset of transonic flow (Fig. 2b).

3.2 *Lifting Test Case*

The validation of the present formulation in lifting forward flight conditions will require many test cases. No single test case will be able to assess the ability of the formulation in predicting the wake structure and circulation, blade pressures and loads, and induced velocities. Even experiments that are specifically designed for code validation often can deal with only one or two of these issues adequately.

This paper is the first attempt to check the formulation in terms of induced velocities. The test case chosen refers to a series of experiments performed at NASA Langley Research Center in 1988 on a model rotor/fuselage configuration [7]. Measurements of the induced velocity were made at azimuthal increments of 30°, at approximately one chord above the tip-path-plane. Although the experiment is for a rotor/fuselage configuration, the calculations have been performed on the isolated rotor. The four-bladed rotor is fully articulated. The blades are of rectangular planform, NACA 0012 airfoil distribution, and $-8°$ linear twist. Comparisons are made with the experiment and with ONERA calculations on the isolated rotor [8] using Eurocopter France's lifting-line rotor code METAR [9, 10]. The METAR code is a classical lifting-line rotor code which models the blades as lifting lines about the quarter-chord point and the wake as a vortex lattice. The induced velocities are calculated using the Biot and Savart law and the lift is calculated from steady two-dimensional airfoil tables. The Kutta-Joukowski theorem then helps determine the circulation. Blade motion is calculated simultaneously by coupling with the blade dynamics code R85 developed by Eurocopter France.

	$\mu = 0.15$				$\mu = 0.23$				$\mu = 0.30$			
	θ_o	A_1	B_1	a_o	θ_o	A_1	B_1	a_o	θ_o	A_1	B_1	a_o
EXPER.	9.37	-1.11	3.23	1.50	8.16	-1.52	4.13	2.00	10.31	-1.55	5.88	2.13
ISOL. ROTOR	7.00	-2.44	2.45	1.97	7.05	-2.20	3.69	1.94	8.21	-2.19	5.11	1.90

Table 1. Trim condidions for lifting test cases.

At present, our code does not include a rotor trim loop, but uses input control geometry. Table 1 gives the trim conditions for the experimental rotor/fuselage configuration and for the isolated rotor as computed by ONERA using R85/METAR. Calculations have been performed using ONERA's trim conditions. Each blade was discretized using 12 panels in the chordwise direction and 8 panels in the spanwise direction. At every time step the wake was held at 2 spirals so as to keep the computational effort per time step constant after 2 revolutions of the rotor. A constant

time step was used which gave azimuthal increments of 20°. A classical skewed-helix wake, traced by the trailing edge line of the non-articulated rotor, was used in all the calculations. The calculations were carried out up to 10 rotor revolutions at which point the velocity potential at any point in the field can be computed using Eq. (2) from known values on the blades and on the wake. The z-component of the induced velocity, $v_z = \partial\phi/\partial z$, was computed on the plane above the rotor by a finite difference expression.

Figures 3-5 present the contour plots of the induced inflow ratio, $\lambda = v_z/V_{tip}$, at the advance ratios 0.15, 0.23, 0.30 respectively.
At $\mu = 0.15$, the present formulation (Fig. 3b) slightly overestimates the region of upwash in the front part of the rotor disc while METAR (Fig. 3c) underestimates this region of upflow and presents a second region of upflow in the rear part of the rotor disc that is neither present in the experiment (Fig. 3a) nor in BEM. The presence of the concentrated tip vortices and rollup of the wake structure can be seen on both sides of the rotor disc in the regions of high gradients (fig. 3a) and is not captured by BEM and METAR since there is no wake rollup in their wake modeling.
At $\mu = 0.23$, the situation is much the same except that the region of upflow is much larger (Fig. 4a). The region of upflow grows in BEM but not in METAR. It is expected that at this advance ratio the fuselage effects are beginning to become important.
At $\mu = 0.30$, the region of upflow is even larger and only BEM (Fig. 5b), considering that there are no fuselage effects, tends in the right direction. At this advance ratio it is interesting to note the similarities between an incompressible calculation of the present formulation (Fig. 5c) and METAR (Fig. 5d). This might be an indication that METAR and other classical lifting-line rotor codes may not be "fully" compressible. In fact, Hoad et al. [11] presented the results of CAMRAD and of several UTRC lifting-line rotor codes which at $\mu = 0.30$ have a behavior similar to METAR. In the same paper it was noticed that for all three advance ratios the analytical methods predicted the maximum downwash on the retreating side of the rotor disc. Figures 3-5 show that the experimental results, BEM and METAR all have the maximum downwash in the rear portion of the disc and skewed to the advancing blade side.

Figure 6 shows the azimuthal variation of the induced inflow ratio at various radial stations for $\mu = 0.30$. The greatest differences between the experimental and numerical results occur where the influence of the fuselage is strong. In the front part of the rotor disc ($\psi = 180°$) the discrepancy is largest at r/R = 0.20, due to the proximity of the hub and cowlings, and is reduced toward the tip. In the rear part ($\psi = 0°$), the largest discrepancies are again at r/R=0.20. METAR calculations with fuselage effects [10] have shown an improvement over isolated calculations especially at $\psi = 180°$ at the inboard stations. At $\psi = 0°$ the inboard stations fall within a region of separated flow due to the hub and upper cowlings and the inviscid calculations, even with fuselage effects, are not able to model this region correctly.

Contour plots of the circulation at $\mu = 0.30$ are shown in Fig. 7. The compressibility effects are limited to the advancing blade side of the disc. In fact, the incompressible solution is similar to METAR on the advancing side while both the compressible and incompressible solutions are rotated by approximately 60° with respect to METAR on the retreating side of the disc. Figure 8 shows the radial distribution of circulation at 90° azimuth. Although the incompressible calculation predicts stronger circulation over the blade span, it is very similar to METAR. The compressible solution is much stronger and reaches its maximum further inboard. Experimental results [12] are also presented at $r/R = 0.60$ where CAMRAD calculations predicted the maximum circulation. No definitive conclusions can be drawn from a single data point along the span. It is hoped that a complete survey of the circulation on the rotor disc will become available for all three advance ratios so as to continue the validation process.

4. CONCLUDING REMARKS

The initial validation of a boundary integral formulation for the aerodynamic analysis of an isolated rotor in forward flight has been presented. Two test cases have been used; one for nonlifting conditions and one for lifting conditions. In the nonlifting case, comparisons with the finite difference method have confirmed the ability of the method to obtain accurate pressure distributions over most of the rotor disc where the flow is linear. The integral formulation is not able to capture the nonlinear effects on the advancing blade tip. In the lifting case, the method has been compared to an industrial lifting-line rotor code for an isolated rotor and experimental data for a rotor/fuselage configuration. There is a good agreement with the experiment in regimes where the fuselage effects are small. At a high advance ratio, $\mu = 0.30$, the solution of the lifting-line rotor code is surprisingly similar to that of the incompressible BEM especially on the advancing blade side of the rotor disc. This is an indication that classical lifting-line rotor codes may not be "fully" compressible.

Considering the recent development of this boundary integral formulation, the present validation exercise has produced satisfactory results. The coarse discretization used in the lifting case has proven to be adequate for calculating induced velocities but finer blade and wake discretization is probably required to obtain accurate pressure distributions on the blades. The classical skewed-helix wake is adequate only at high advance ratios. At low advance ratios, a prescribed wake with tip vortex modeling needs to be introduced in the code and eventually a free wake model. A rotor trim loop needs to be included in the code so as to make it independent of input control geometry.

An exciting feature of the present formulation is that the inclusion of the fuselage is straightforward and results in a fully unsteady global calculation. Encouraged by the preliminary results presented in this paper, we intend to continue developing the formulation and apply it to a number of rotorcraft interactional aerodynamics problems.

ACKNOWLEDGEMENTS

This work was partially supported by the European Economic Community under the BRITE/EURAM Contract No. AERO-0011-C(A) "Helicopter Rotor/fuselage Interactional Aerodynamics", acronym SCIA. The authors would like to thank A. Desopper and N. Bettschart of ONERA for providing their results obtained from the rotor code METAR developed by Eurocopter France.

REFERENCES

1. L. Morino and K. Tseng, **A general theory of unsteady compressible potential flows with applications to airplanes and rotors**. Eds: P.K. Banerjee and L. Morino, Developments in Boundary Element Methods, Volume 6: Nonlinear Problems of Fluid Dynamics. Elsevier Applied Science Publisher, Barking, UK. 1990.

2. M. Gennaretti, O. Macina, and L. Morino, **A new integral equation for potential compressible aerodynamics of rotors in forward flight**, Proceedings of the International Specialist's Meeting on *Rotorcraft Basic Research*, Atlanta, U.S.A., March 1991.

3. L. Morino, M. Gennaretti, and P. Petrocchi. **A general theory of potential aerodynamics with applications to helicoper rotor-fuselage interaction**, Symposium of the International Association for Boundary Element Methods. Kyoto, Japan, Oct. 1991.

4. H. Tai and L. H. Runyan, **Lifting surface theory for a helicopter rotor in forward flight**, NASA TM-86315, Sept. 1984.

5. J. J. Philippe and J. J. Chattot, **Experimental and theoretical studies on helicopter blade tips at ONERA**, Sixth European Rotorcraft and Powered Lift Aircraft Forum, 1980.

6. A. Pagano, **UTAH - Unsteady transonic aerodynamics of helicopters, vol. I - nonlifting calculations**, CIRA Report DILC-INT-TR-278, July 1992.

7. J. W. Elliott, S. L. Althoff, and R. H. Sailey, **Inflow measurement made with a laser velocimeter on a helicopter model in forward flight: volumes I-III - rectangular planform blades at an advance ratio of 0.15, 0.23, 0.3**, NASA TM- 100541-3, 1988.

8. A. Desopper, Private communications, 1991.

9. W. G. Bousman, C. Young, N. Gilbert, F. Toulmay, W. Johnson, and M. J. Riley, **Correlation of Puma airloads - lifting-line and wake calculations**, Fifteenth European Rotorcraft Forum, 1989.

10. A. Dehondt and F. Toulmay, **Influence of fuselage on rotor inflow performance and trim**, Fifteenth European Rotorcraft Forum, 1989.

11. D. R. Hoad, S. L. Althoff, and J. W. Elliot, **Rotor inflow variability with advance ratio**, 44th Annual Forum of the American Helicopter Society, Washington, D.C., June 1988.

12. D. R. Hoad, **Helicopter local blade circulation calculations for a model rotor in forward flight using laser velocimeter measurements**, 47th Annual Forum of the American Helicopter Society, Phoenix, U.S.A., May 1991.

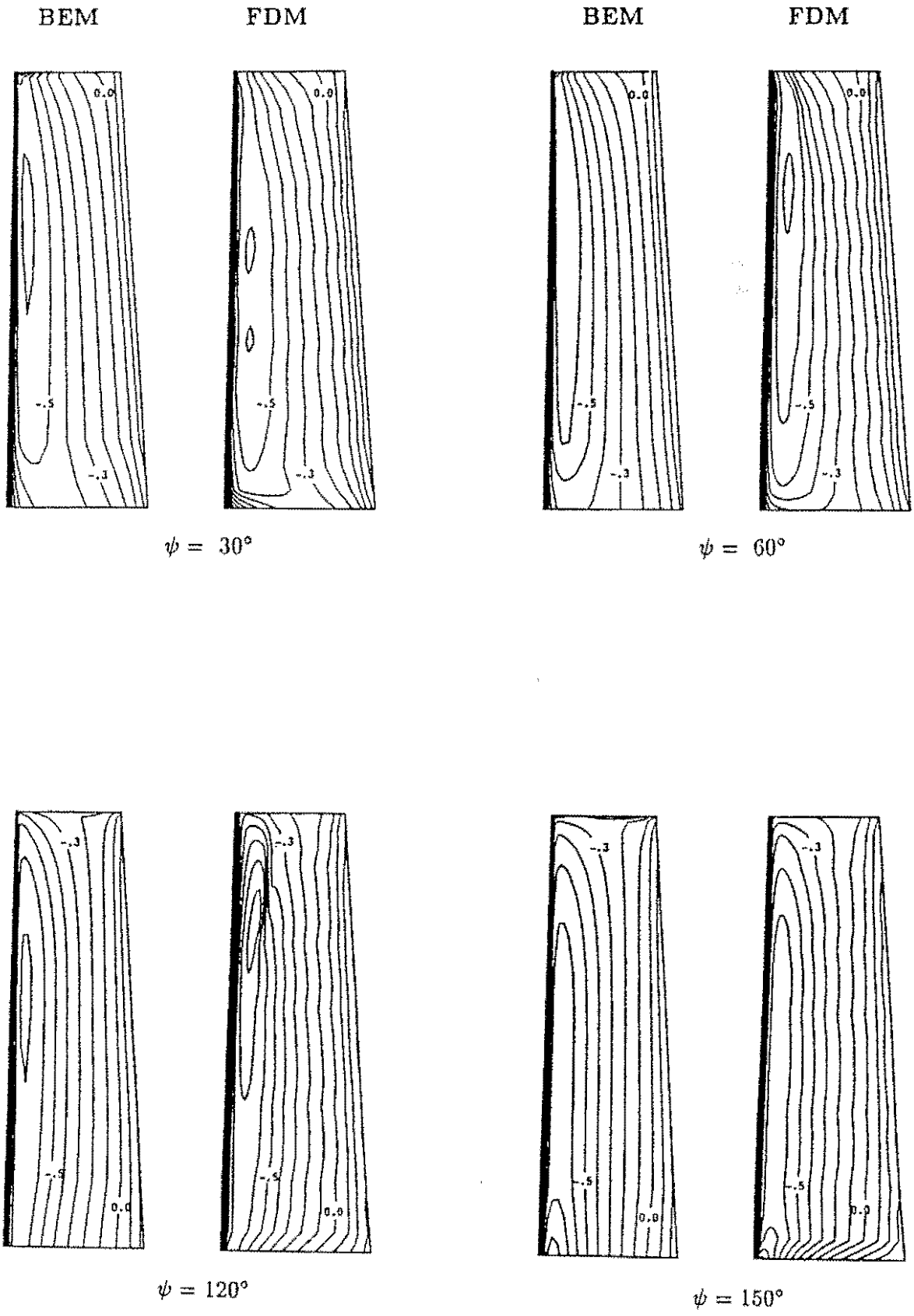

Figure 1. Iso-pressure coefficient lines on the nonlifting blade at four azimuthal stations. Comparison of the present formulation (BEM) with the finite difference method (FDM).

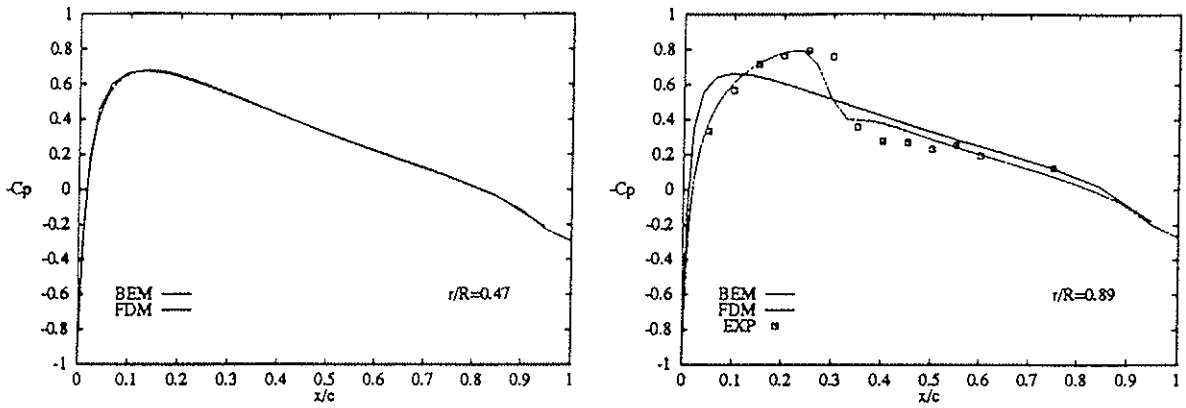

Figure 2. Pressure coefficient distribution on the nonlifting blade at $\psi = 120°$ for the radial stations r/R = 0.47, 0.89.
Comparison of the present formulation (BEM) with the finite difference method (FDM).

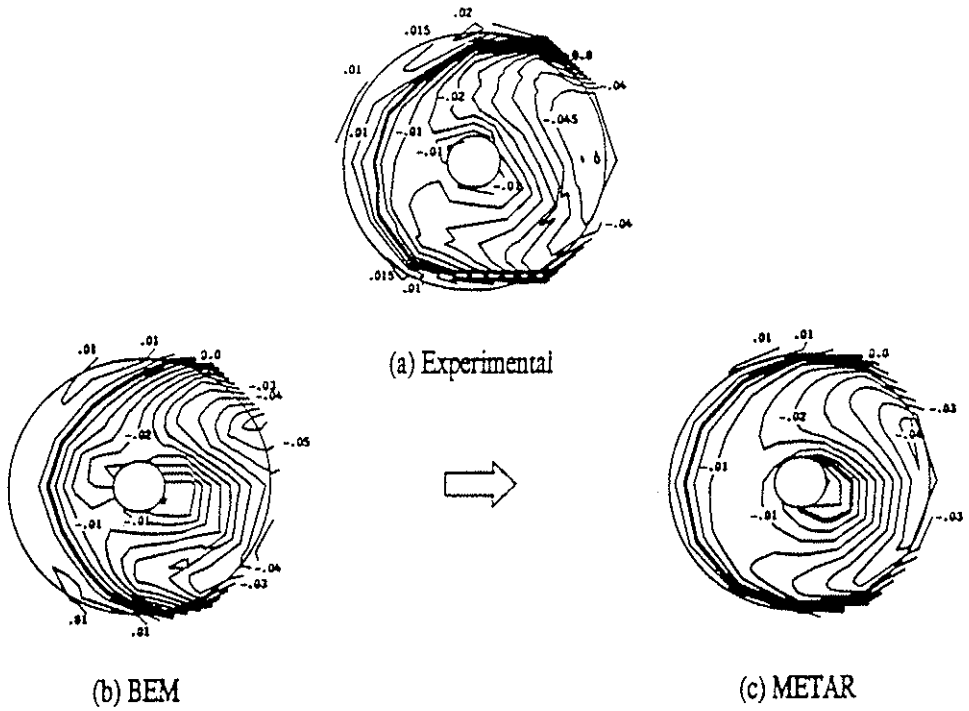

Figure 3. Contour plots of the induced inflow ratio above the tip-path-plane at $\mu = 0.15$.
Comparison of the present method (BEM) with measurements and a lifting-line code (METAR).

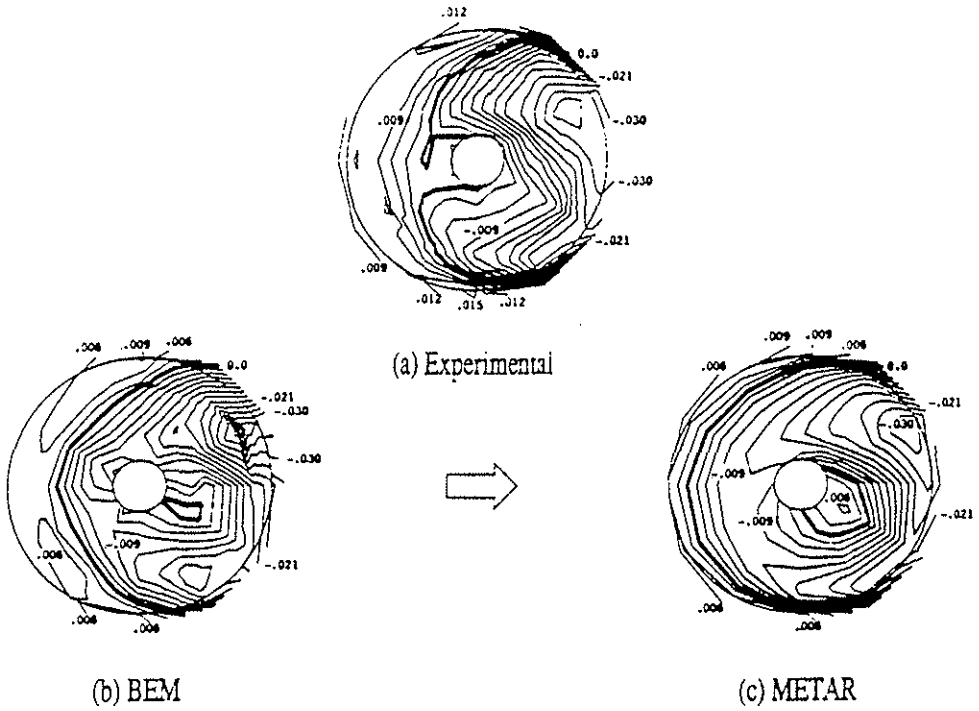

Figure 4. Contour plots of the induced inflow ratio above the tip-path-plane at $\mu = 0.23$. Comparison of the present method (BEM) with measurements and a lifting-line code (METAR).

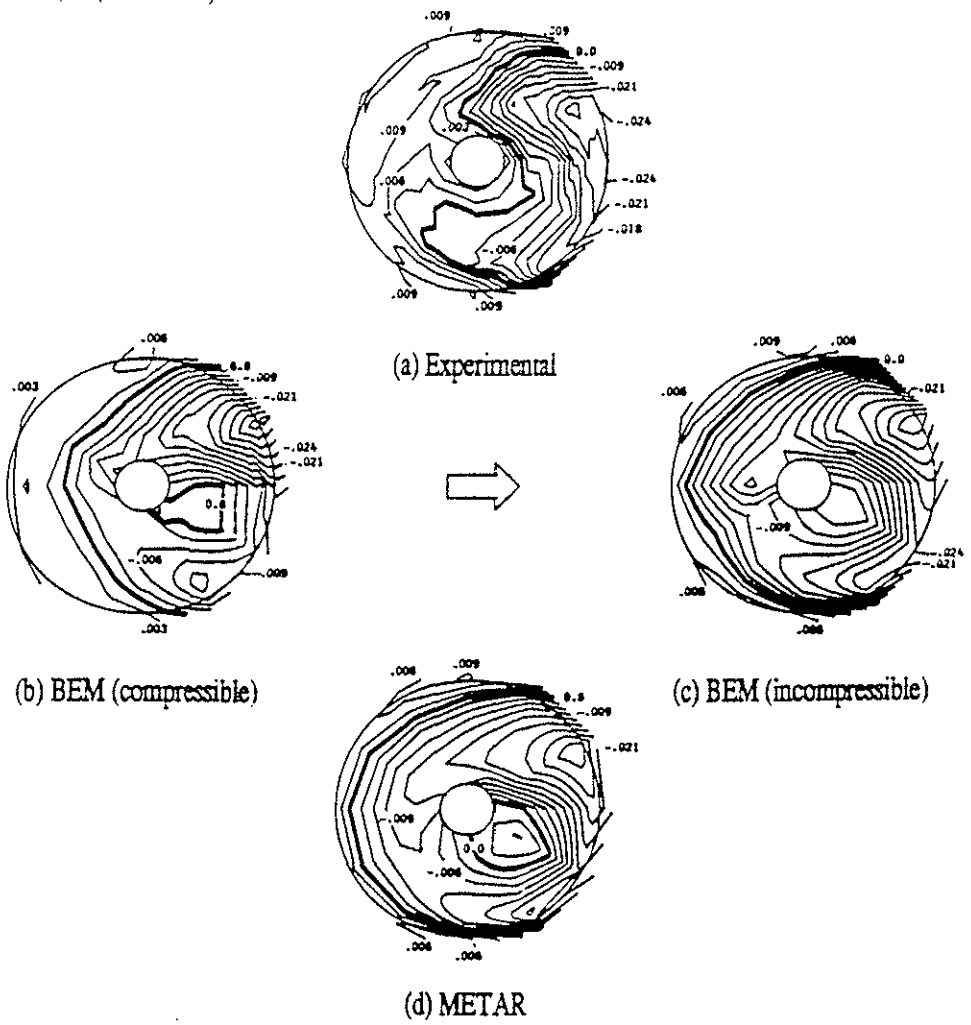

Figure 5. Contour plots of the induced inflow ratio above the tip-path-plane at $\mu = 0.30$. Comparison of the present method (BEM - both compressible and incompressible calculations) with measurements and a lifting-line code (METAR).

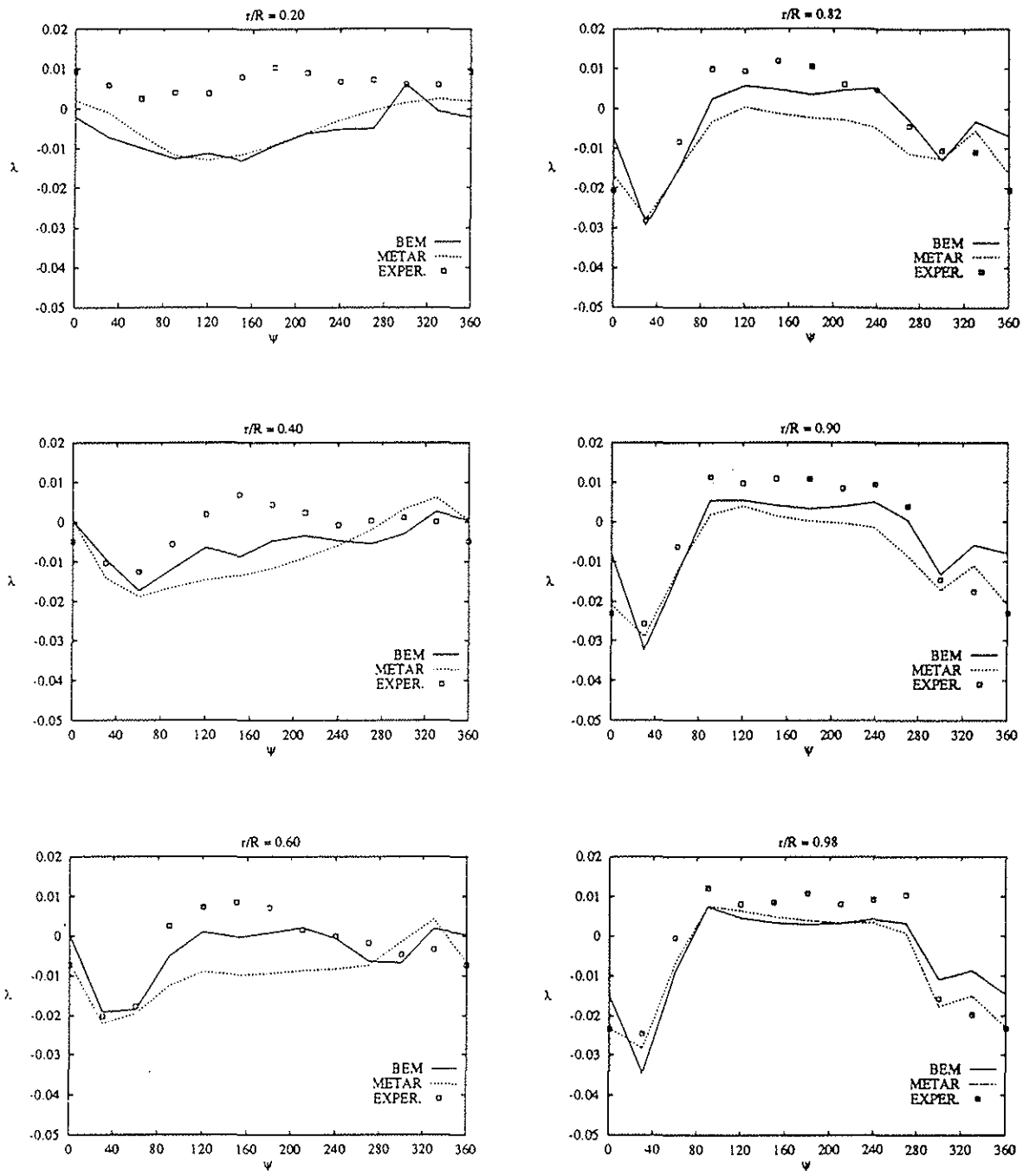

Figure 6. Azimuthal distribution of the induced inflow ratio at $\mu = 0.30$. Comparison of the present method (BEM) with measurements and a lifting-line code (METAR).

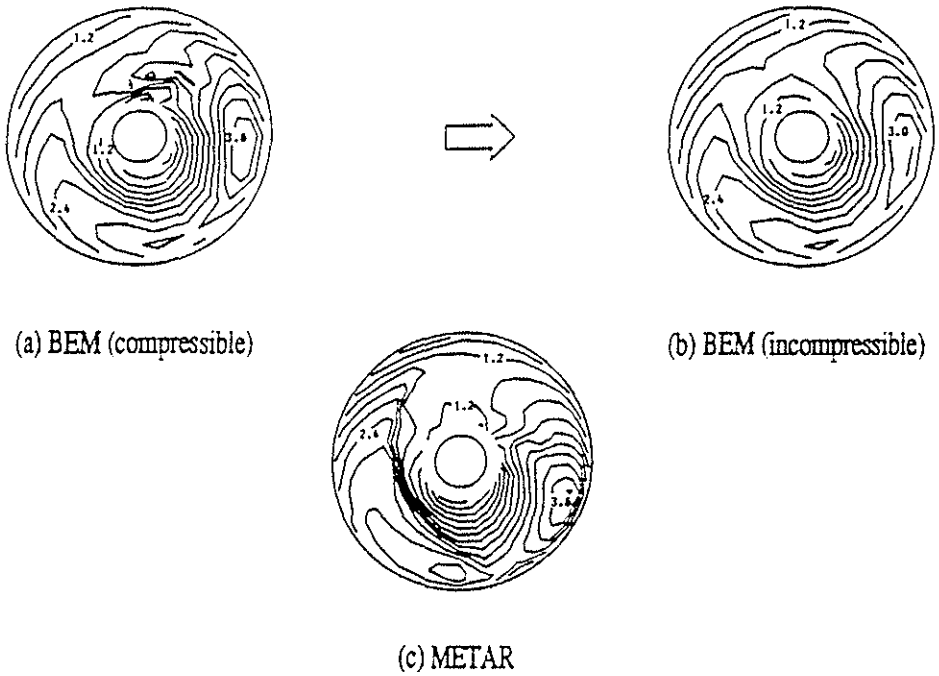

Figure 7. Contour plots of the circulation at $\mu = 0.30$. Comparison of the present method (BEM - both compressible and incompressible calculations) with a lifting-line code (METAR).

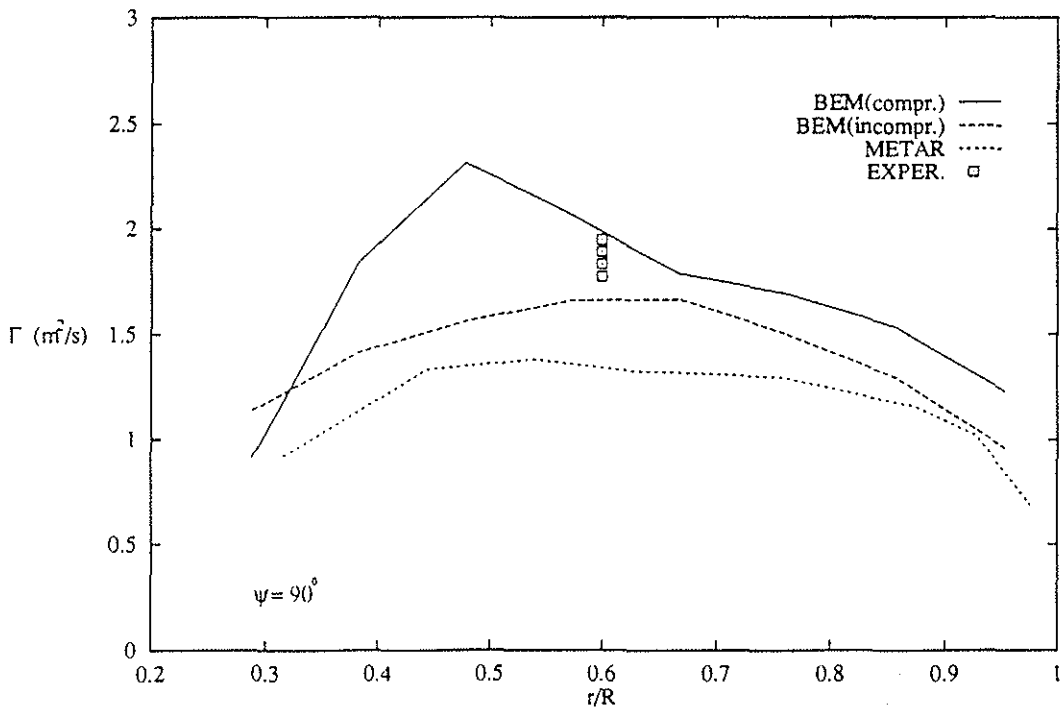

Figure 8. Azimuthal distribution of the circulation at $\mu = 0.30$, $\psi = 90°$. Comparison of the present method (BEM - both compressible and incompressible calculations) with a lifting-line code (METAR) and with an experiment [12].